EXPERIMENTAL RESULTS IN PION-NUCLEON SCATTERING: QCD SYMMETRY TESTS

H. J. Leisi

ETH Zürich, Institute for Particle Physics
ETH Hönggerberg / HPK F 24
8093 Zürich

Abstract

We present the values of the πN s-wave scattering lengths as deduced from the pionic-hydrogen X-ray experiments. Comparison with Chiral Perturbation Theory (ChPT) shows that the scattering lengths are dominated by the first-order contribution (current-algebra limit). From the isovector scattering length b_1 (using the GMO sum-rule) a new value of the πN coupling constant is obtained ($g_{\pi NN} = 13.11 \pm 0.09$), and from this the Goldberger-Treiman discrepancy is found to be $\Delta_{GT} = (1.9 \pm 0.8)10^{-2}$. This result invalidates an objection against the standard form of ChPT. The new value of the isoscalar scattering length b_0 leads to an increase of the πN sigma-term by about 7 MeV, while the extended tree-level (ETL-) model indicates an increase of about 12 MeV, with respect to the value from the Karlsruhe-Helsinki (KH) data. Constraints on the scattering lengths in a (b_0, b_1) plot are used to test isospin symmetry of the strong interaction. The projection to threshold of the analysis of low-energy $\pi^{\pm}p$ elastic scattering data using the ETL-model disagrees in b_1 with the measured value by 11 ± 2 %. This implies that the isospin symmetry of the strong interactions is explicitly broken, or the ETL-model has a (small) missing piece, or both.

1. Introduction

Experiments probing the low-energy πN interaction have reached precisions which are unique in hadron physics. The development of heavy-baryon chiral perturbation-theory in recent years offers now the possibility to investigate basic symmetry properties of QCD, namely the explicit breaking of chiral- and isospin symmetry.

QCD reveals the *spontaneous breakdown of chiral symmetry* (also referred to as „*hidden symmetry*“): The ground state is less symmetric than the hamiltonian of the theory. In QCD with massless u- and d-quarks the hamiltonian is symmetric with respect to the chiral symmetry group $SU(2)_R \times SU(2)_L$, which breaks down to the SU(2) isospin-symmetry group in the ground state [1]. As a consequence of Goldstone's theorem, there are then three *massless* Goldstone bosons (π^+,π^o,π^-) in the ground state. In a next step, the (small) u- and d-quark masses are turned on and ChPT is used to calculate the properties of the low-energy strong interactions, e.g. the π*N scattering lengths.*

It is the task of the experimentalist to measure precisely the (low-energy) properties of the pion interactions. The goal of the game is then to test – by means of ChPT – the *symmetry structure of QCD* which manifests itself only at *low energies*.

2. Results from the pionic hydrogen experiment

2.1 The experiment

The idea of the experiment is to measure precisely the 3p - 1s X-ray transition in pionic hydrogen, determining both, the (average) transition energy and the line width (Fig. 1). We then calculate the purely electromagnetic 3p - 1s transition energy, subtract from it the measured energy and obtain the strong-interaction level-shift ε_{1s} of the 1s state (shift and width of the 3p state are negligibly small). This quantity is a measure of the s-wave π^-p elastic scattering amplitude at threshold. The measured line width is dominated by the decay width Γ_{1s} of the 1s ground state, resulting from the single-charge-exchange (SCX) and the decay into (γ n) (Fig. 1). Using the known relative yield of the two decay processes (the Panofsky ratio), we can express the width in terms of the square of the SCX amplitude at threshold [2] [3] [4]. We have also measured the strong-interaction shift and the width of the 1s ground-state of the pionic *deuterium* atom [5] [6]. In this way we obtain the π^-d scattering length (real and imaginary part). The real part can be related by three-body calculations to (essentially) the isoscalar πN scattering length b_0. The experiment as a whole, therefore, leads to three independent constraints on the πN scattering length (see sect. 2.2).

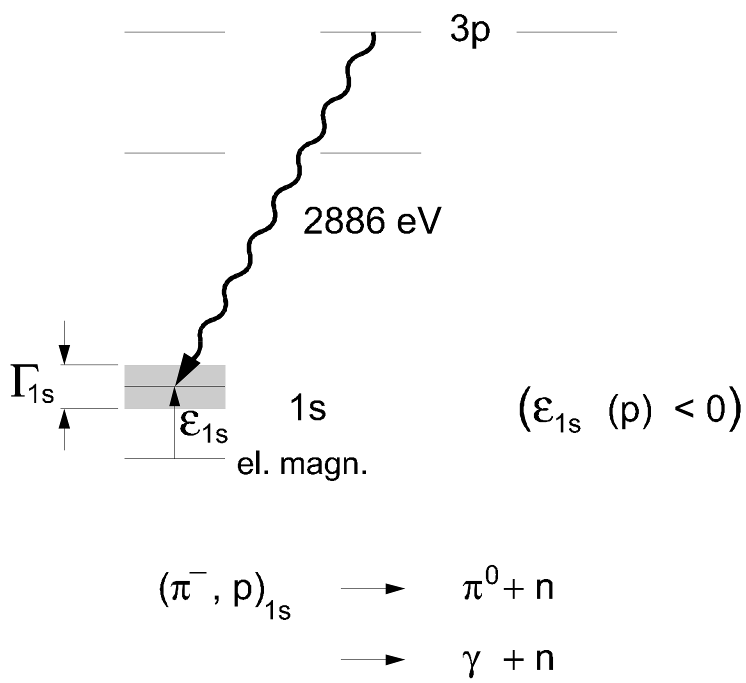

Fig. 1: Pionic hydrogen 3p - 1s X-ray transition and decay of the 1s ground state.

How does one produce pionic hydrogen? This is very easy – as long as you have a π^- beam: The pions are slowed down in matter (particularly in hydrogen), until they reach the velocity of

$$v_{\pi^-} \approx \sqrt{\frac{m_e}{m_\pi}} \cdot v_{e^-} \ , \tag{1}$$

where v_e^- is the (semi-classical) velocity of the electron in the ground state of hydrogen (m_e, m_π are the masses of electron and pion) (Fig. 2). Eq. (1) gives the velocity of the pion in a pionic Rydberg-atom state whose radius is equal to the Bohr radius a_B of electronic hydrogen. At the velocity (1) a resonance-type process therefore occurs by which the electron of hydrogen (at the distance a_B) is replaced by the negative pion, forming pionic hydrogen in the highly excited state with

$$n \approx \sqrt{\frac{m_\pi}{m_e}} \approx 17 \, . \tag{2}$$

It is obvious that for this process energy and angular momentum (in the high-mass limit of the proton) are conserved (Fig. 2). The pion of the highly excited state then cascades down by various atomic processes until it reaches the low-energy states from which X-ray decay dominates in a low-density (gaseous) hydrogen environment [4].

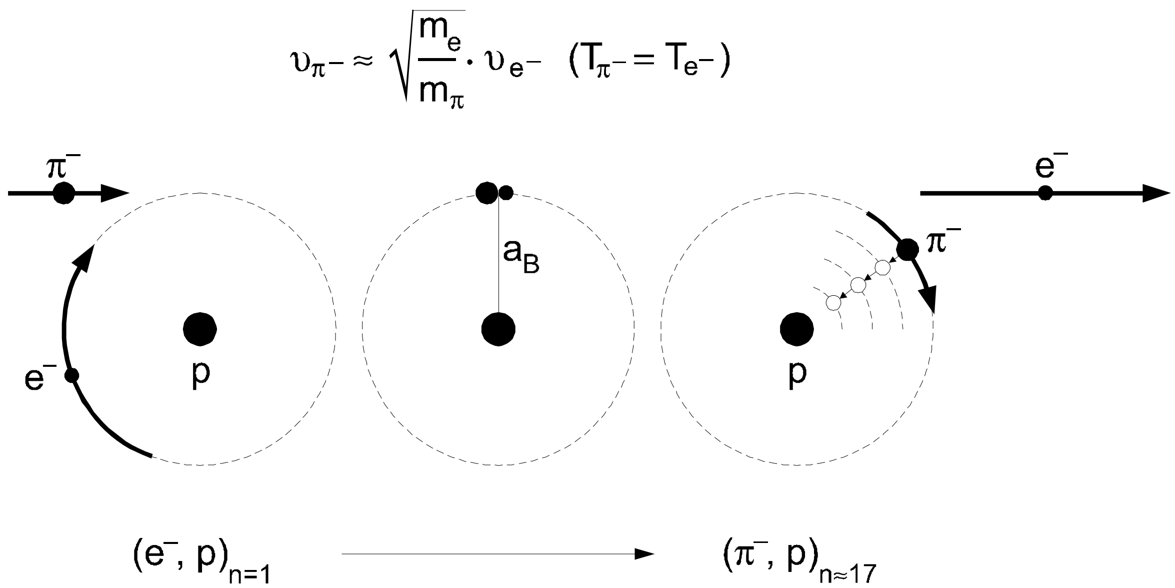

Fig. 2: Formation of a pionic atom in a Rydberg-state, starting from electronic hydrogen.

The experimental set-up is sketched in Fig. 3. For all kinds of (important) details we refer to the papers cited above and references therein. Pions from the πE5 beam at PSI are degraded inside the cyclotron trap which is a magnetic field device designed to increase the stop density in the target cell at its center. The X-rays from the target cell are measured with two bent-crystal spectrometers mounted on top of each other (with three quartz （110） crystals each). The X-ray detector system consists of an array of CCD's with a total of 3.6 million pixels. The signature for a (2.9 keV) X-ray is a single pixel event with the corresponding amount of energy deposited. In addition to the cryogenic gaseous H_2 target-cell (15 bar equivalent), an argon electronic X-ray source for energy calibration and one for stability monitoring (Ar in Fig. 3) and a beryllium pionic X-ray target for measuring the spectrometer resolution curve (Be in Fig. 3) are used.

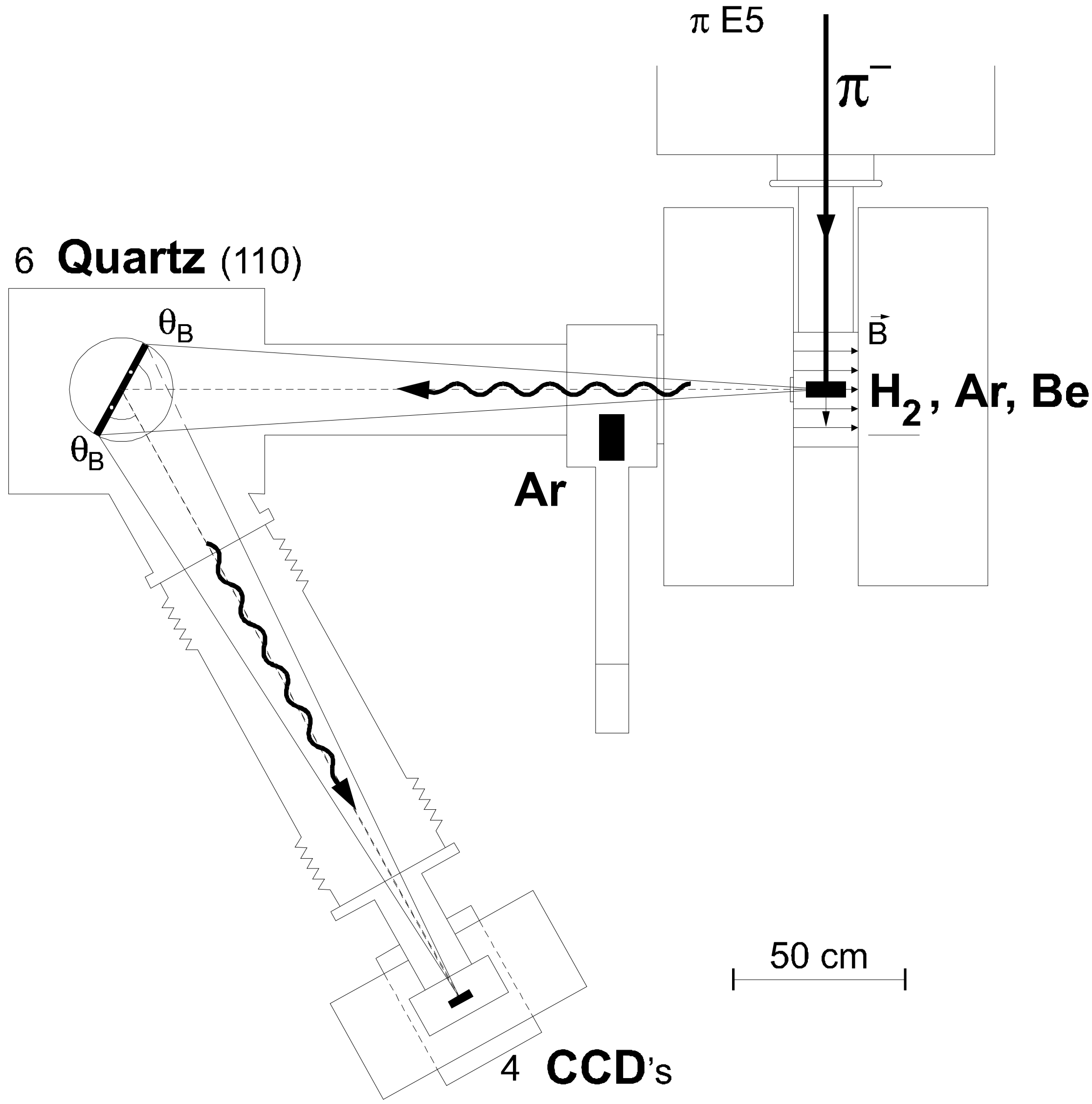

Fig. 3: Layout of pionic hydrogen experiment at PSI.

Fig. 4 shows the 3p - 1s pionic hydrogen (π^-p) X-ray spectrum together the electronic argon (Ar K_α) X-ray lines and the pionic 4f - 3d (π^-Be) X-ray line. The broadening of the 3p - 1s X-ray line is clearly visible (comparing Fig. 4 （a） with （c）).

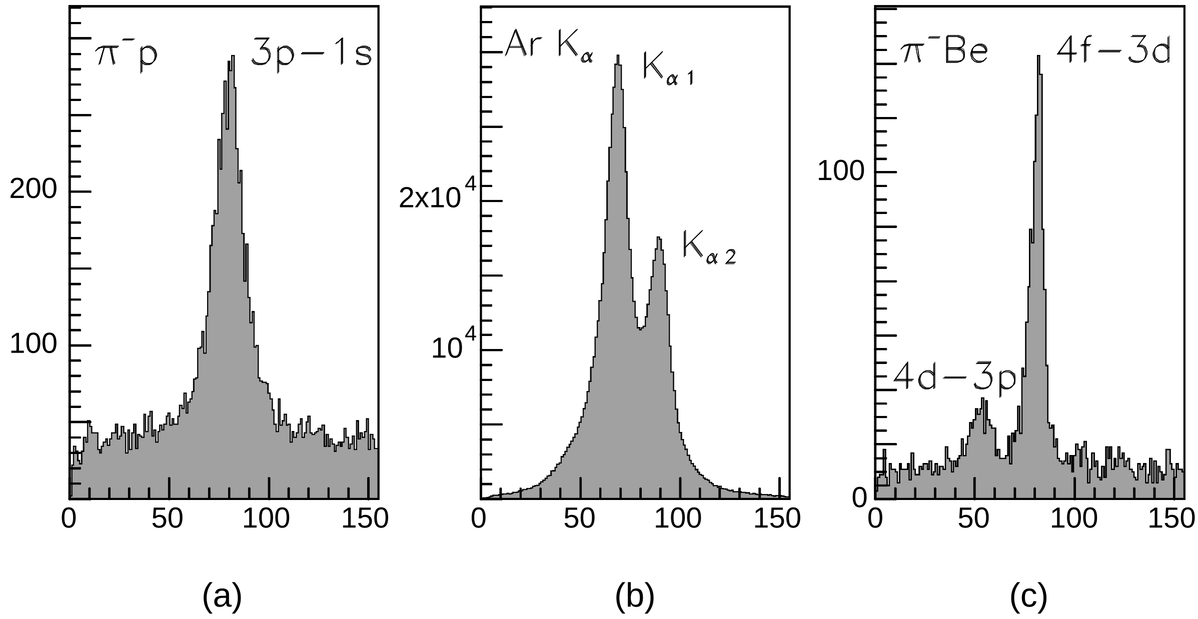

Fig. 4: X-ray spectra of the pionic hydrogen experiment (counts per channel) [4]: (a) pionic hydrogen 3p - 1s transition; (b) electronic argon K_α transitions; (c) pionic beryllium 4f - 3d transition.

In order to arrive at the strong-interaction shift ε_{1s} we have to calculate the electromagnetic transition energy (in the absence of the strong interaction). Table 1 shows the electromagnetic binding energy of the 1s state of pionic hydrogen [7]. The main uncertainty stems from the error in the pion mass (point-Coulomb energy). The total uncertainty of 9 meV is well below the uncertainty quoted in ε_{1s} (47 meV) [4].

Electromagnetic binding energy of 1s state [eV] [7].		
Point-Coulomb (Klein-Gordon)	3'235.156	(8)
Coulomb finite size (proton, pion)	-0.102	(3)
Vacuum polarization, order α^2 (Uehling potential; finite size)	3.246	(1)
HORC:		
– relativistic recoil	-0.047	
– vacuum pol., order α^3 – vertex correction (order α^2)	0.011	(3)
total binding energy	3'238.264	(9)

Table 1

In Fig. 5 we show the various determinations of ε_{1s} for pionic hydrogen as a function of time [8] [9] [10] [11] [2] [3] [4]. The first measurement of our group (Beer, 91) is compatible with the present value (Schröder, 96) whose precision is better than 1%. Fig. 6 shows the same for ε_{1s} of pionic deuterium [12] [8] [10] [5] [6]; the strong-interaction shift is now known to 4% (Chatellard, 95).

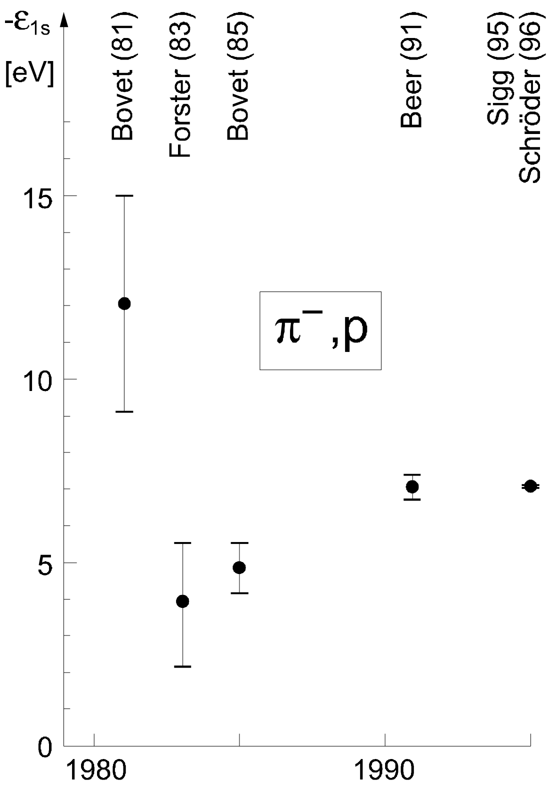

Fig. 5: Strong-interaction shift measurements for pionic hydrogen as a function of time. The present value is ε_{1s} = -7.11 ± 0.05 eV [4].

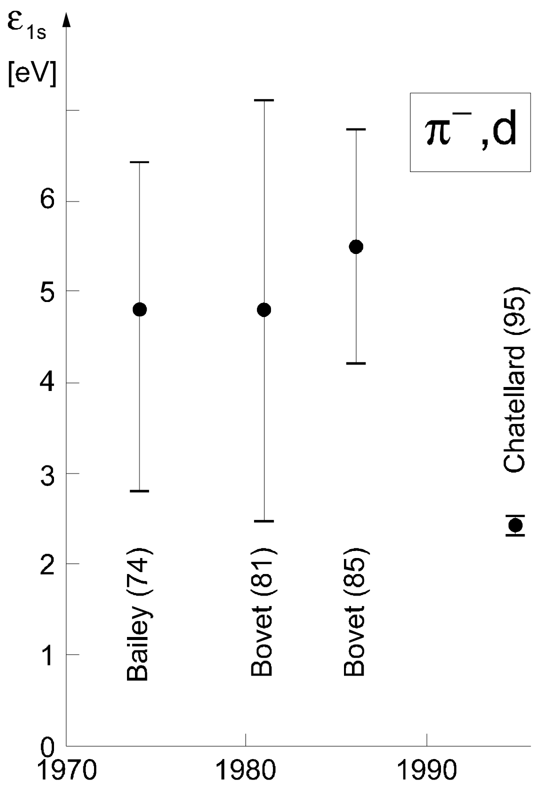

Fig. 6: Strong-interaction shift measurements for pionic deuterium as a function of time. The present value is ε_{1s} = 2.43 ± 0.10 eV [6].

2.2 Scattering lengths and isospin-symmetry test

The pionic-hydrogen level shift ε_{1s} is not yet a purely hadronic quantity. If the strong interaction is switched on, then the strong potential modifies the electromagnetic interaction and changes the transition energy slightly. There is, in addition, the so-called mass-splitting effect: Final states of the π^on system (and the γ n system) modify the 1s bound state. We have calculated all these so-called *electromagnetic corrections* [7]; they change ε_{1s} of hydrogen by (2.1 ± 0.5)% (about twice the quoted error in ε_{1s}). From the corrected shift we obtain the s-wave πN scattering amplitude [4]

$$a_{\pi^-p\to\pi^-p} = b_0 - b_1 = \left(0.0883 \pm 0.0002 \pm 0.0006\right) m_\pi^{-1} , \tag{3}$$

$$\left(b_0 \equiv a^+_{0+} \quad ; \quad b_1 \equiv -a^-_{0+}\right)$$

where the first error is statistical and the second systematic. In deriving the result (3), isospin symmetry of the strong interaction is assumed.

We now turn to the decay width of the 1s state of pionic hydrogen which is measured for the first time. The line width of the 3p - 1s X-ray transition has to be corrected for Doppler effect, resulting from the preceding atomic cascade transitions [4]. One obtains the decay width

$$\Gamma_{1s} = 0.865 \; \pm \; 0.067 \, \mathrm{eV} \; , \tag{4}$$

and the corresponding SCX amplitude

$$a_{\pi^- p \to \pi^0 n} = \sqrt{2} \cdot b_1 = -0.127 \pm 0.006 \;\; m_\pi^{-1} \; . \tag{5}$$

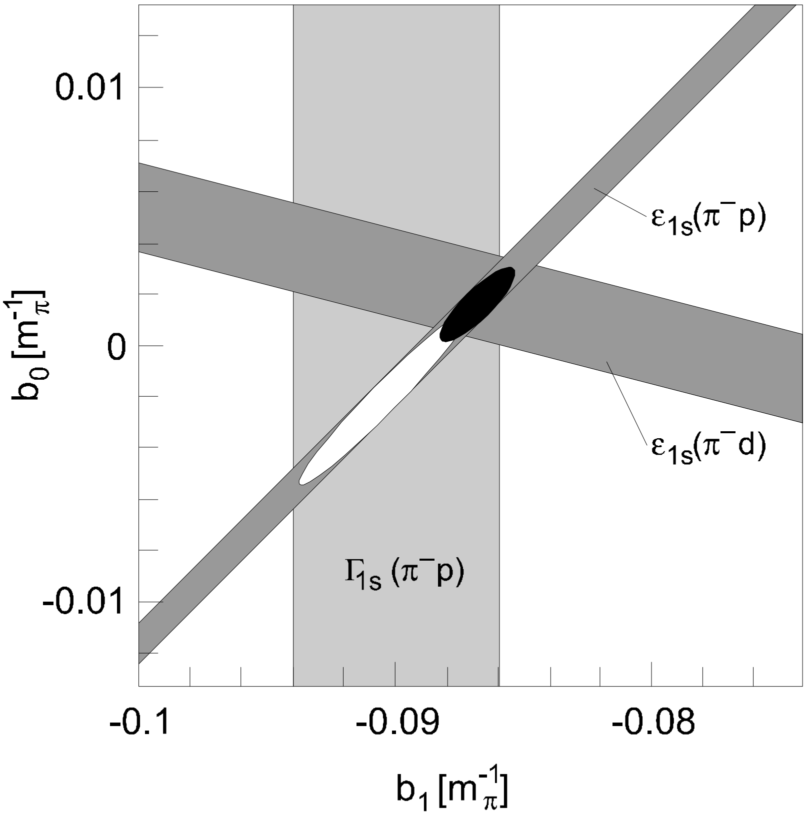

Fig. 7: Constraints on the πN scattering lengths b_0 and b_1 from the pionic hydrogen shift and width measurements and the pionic deuterium shift measurement.

The two constraints (3) and (5) on the scattering lengths b_0, b_1 are plotted in Fig. 7 ($\varepsilon_{1s}\,(\pi^- p)$ and $\Gamma_{1s}\,(\pi^- p)$); the white ellipse corresponds to the one-standard-deviation contour. Also shown in Fig. 7 is the constraint derived from the strong-interaction shift ε_{1s} of pionic *deuterium* ($\varepsilon_{1s}\,(\pi^- d)$) [6]. This band is based on 3-body calculations by Thomas and Landau [13]. The main uncertainty of the band originates from the estimated theoretical uncertainties and not from our experiment [1) 2)]. The dark ellipse in Fig. 7 is the contour from all three constraints. The corresponding scattering lengths are:

$$b_0 = \left(1.6 + 1.3\right) \times 10^{-3} \; m_\pi^{-1} \tag{6}$$

$$b_1 = -\left(86.8 \pm 1.4\right) \times 10^{-3} \, m_\pi^{-1} \; . \tag{7}$$

Note that the two quantities (6) and (7) are correlated as displayed in Fig. 7.

---

1) New calculations are in progress by several groups.

2) The electromagnetic corrections for deuterium are so far incomplete.

The (b_0, b_1) plot of Fig. 7 represents an *isospin-symmetry test of the strong interaction* [14]. This is because the most general, isospin-symmetric interaction at threshold is given by two real numbers (e.g. b_0 and b_1). If we have more than two independent observables (assuming isospin symmetry all along the analyses), then the number of constraints is redundant. Therefore, if the three constraints – originating from independent observables – were incompatible, then isospin symmetry would have to be violated. Since the constraints are compatible (at the level of precision of the experiments), we have in (6) and (7) a precise determination of the (s-wave) πN scattering lengths b_0, b_1.

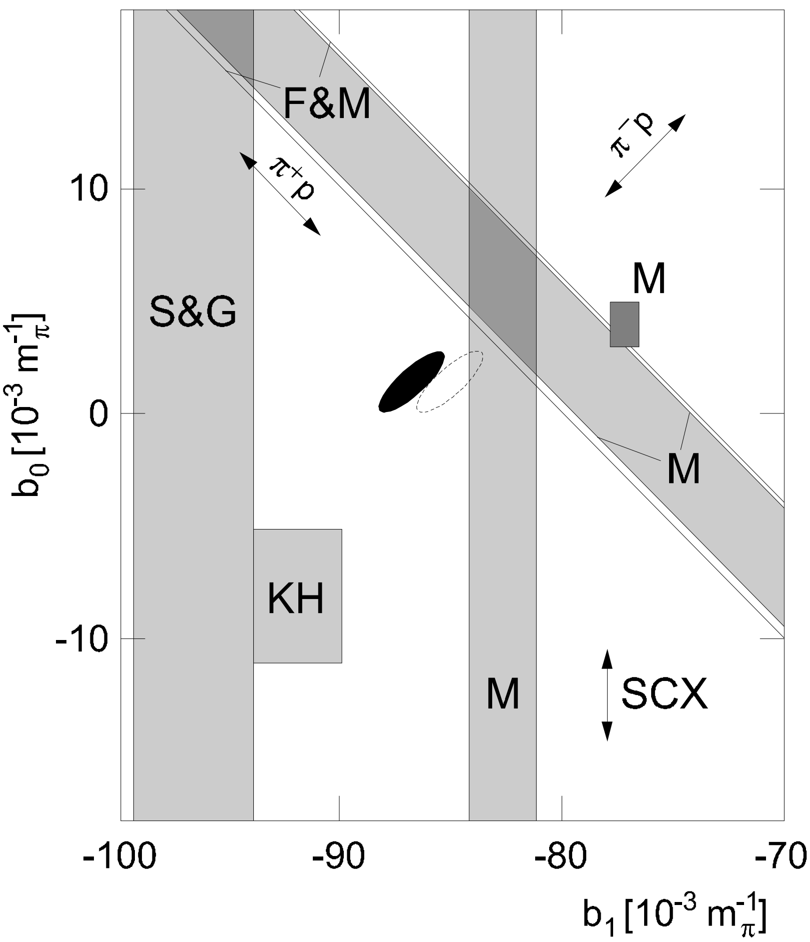

Fig. 8: Constraints on the πN scattering lengths b_0 and b_1 from various measurements and analyses (see text).

Before exploiting this result (see sect. 2.3), we compare the values of the scattering lengths with other recent and frequently quoted determinations and constraints derived from πN data in Fig. 8. First it should be stressed that all determinations – except ours – require some way of extrapolating from higher energies to threshold; our measurements are the only direct determination of the scattering lengths. Taking the results displayed in Fig. 8 at face value, you would conclude that isospin symmetry is strongly violated – provided the incompatible constraints are derived from independent observables. This is not the case e.g. for the two b_1 determinations (S&G) [15] and M(SCX) [16], since they are based essentially on the same SCX data and, hence, should agree. Some problems with the analyses must exist in this case. The potential-model approach of ref. [15] does not implement analyticity and crossing-symmetry. Moreover, the p-wave extrapolation might be incomplete. We therefore disregard S&G in our further discussions. On the other hand, the two constraints F&M [17] and M(π^+p) [16] are derived both from the π^+p elastic scattering data by completely different methods; nevertheless one would expect them to agree – and they do. The square KH is from the Karlsruhe-Helsinki dispersion-relation partial-wave analysis [18], based on experiments conducted before 1980 (the earlier π^+p data are not confirmed). The uncertainties quoted do not include normalization errors. Hence we also disregard the KH prediction of the scattering lengths.

The largest remaining incompatibility clearly is between the square M($\pi^\pm$p) and our ellipse. All constraints marked with M in Fig. 8 are extrapolations from Matsinos' analysis of πN scattering data below 100 MeV pion energy [16]; the values are quoted in part in ref. [23]. This analysis is based on the ETL-model (extended tree-level) of the πN interaction. Provided this model is valid (and the electromagnetic corrections used are correct), we would see a large violation of isospin symmetry of the strong interaction. After having exposed the ETL-model in sect. 3.1 and commented on electromagnetic corrections in sect. 4.2, I will take up the problem of isospin violation in sect. 4.3.

It is claimed that the SP98 partial-wave dispersion-relation solution of the VPI group [19] leads to precise values of the scattering lengths – compatible with our results (6), (7) [20]. The values of the VPI group are not given in ref. [19], however; they are quoted by the authors of ref. [23]. In view of the importance of the problem of isospin-symmetry breaking (see sect. 6.1), one would like to see a detailed discussion of these results (method of analysis, database, realistic error estimates, electromagnetic corrections, etc.).

2.3 Conclusions from theoretical relations

In this section we *assume* isospin-symmetry of the strong interaction to hold and draw conclusions from the results (6), (7).

We first compare the measured scattering lengths with the theoretical expectations of *current-algebra* and *ChPT*. The famous current-algebra prediction of Weinberg is

$$b_0 = 0; \quad b_1 = -\frac{1}{8\pi F_\pi^{\,2}} \; \frac{m_N}{m_N + M_\pi} \cdot M_\pi = -0.0790 \; m_\pi^{-1} \; , \tag{8}$$

where F_π = 92.42 ± 0.26 MeV is the pion decay constant, M_π the (strong-interaction) pion mass, and m_N the nucleon mass. The value for b_1 above is obtained by taking for M_π the charged-pion mass (m_π). Baryon ChPT is a generalization of current-algebra and has recently been evaluated systematically for the πN interaction up to and including 3rd order (work on 4th order is in progress) [21] [22] [23]. The 1st-order result corresponds to the current-algebra limit. Some of the terms of the ChPT expansion depend on a priori unknown low-energy constants (LEC's). In Table 2 we have calculated the LEC's-independent terms of the chiral expansion for b_0, b_1 [22] and compare with the measured values (6), (7). The comparison shows the remarkable result that the *1st-order values are very close to the experimental scattering lengths* (see also Fig. 9). On the other hand, there seems to be a convergence problem of the chiral series – even at threshold where ChPT should work best: The 3rd-order contribution to b_0 e.g. is still large compared to b_0 (Table 2). The experimental values of b_0, b_1 can be used to constrain efficiently the combinations of LEC's which enter the various terms in the expansion.

	1st order	2nd order	3rd order	Experiment $\left[10^{-3} \cdot m_{\pi}^{-1}\right]$
b_0	0	LEC's dependent	8.5	1.6 ± 1.3
b_1	–79.0	0	LEC's dependent	-86.8 ± 1.4

Table 2

Fettes et al. [23] have determined the LEC's from data above threshold and obtained the weak prediction FMS for b_0, b_1 shown in Fig. 9. We would rather recommend to use the experimental values of b_0, b_1 as part of the database for constraining the LEC's (see sect. 6.2).

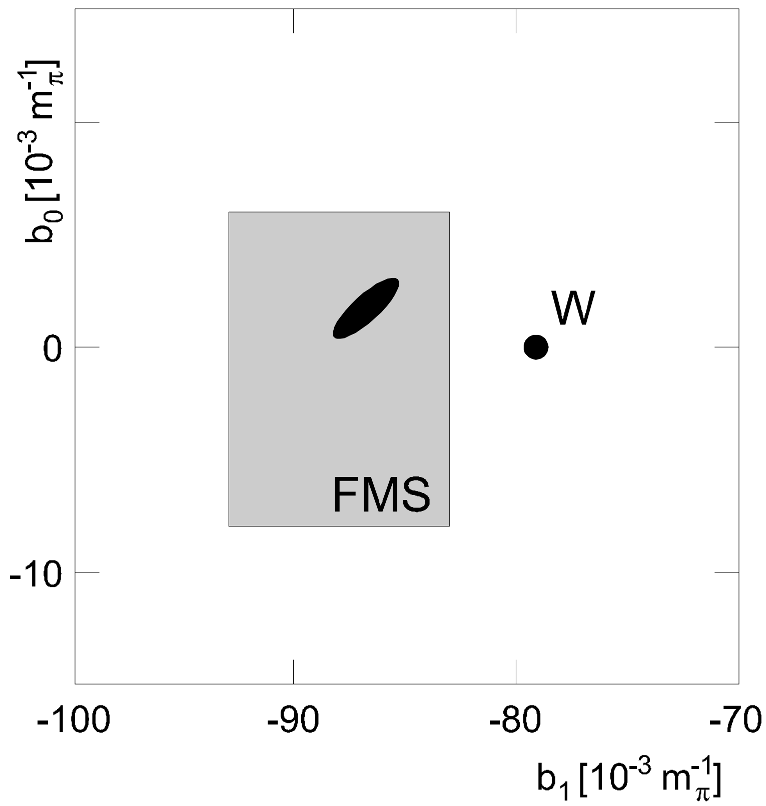

Fig. 9: Constraints on the πN scattering lengths b_0 and b_1 from the pionic hydrogen and deuterium experiments (ellipse), chiral perturbation theory (FMS), and the current-algebra prediction (W).

Second, we determine a new value for the π*N coupling constant* from the isovector scattering length b_1,using the GMO-sum rule. The πN coupling constant f is related to b_1 by [24]

$$\frac{f^2}{4\pi} = -\frac{\left(M_\pi^2 - \nu_B^2\right)\left(m_N + M_\pi\right)}{2\, m_N \cdot M_\pi} b_1 - \frac{M_\pi^2 - \nu_B^2}{2} \cdot J \;, \tag{9}$$

$$\left(\nu_B = -\frac{M_\pi^2}{2 m_N}\right)$$

where

$$J = \frac{1}{4\pi^2} \int_0^{\infty} \frac{\sigma_{\pi^- p} - \sigma_{\pi^+ p}}{\sqrt{q^2 + M_\pi{}^2}} \cdot dq \tag{10}$$

is dominated by the cross sections around the Δ_{33} resonance. For (10) we are using the average of the two values

$$J_{VPI} = -1.041 \text{ mb} ; \qquad J_{KH} = -1.056 \text{ mb}$$

from ref. [25] and obtain with (7)

$$\frac{f^2}{4\pi} = 0.0757 \pm 0.0010 . \tag{11}$$

The value (11) will be compared with other determinations in sect. 3.1 (Table 4).

With the coupling constant (11) we can check the *Goldberger-Treiman relation* reflecting chiral symmetry:

$$g_{\pi NN} = \frac{m_N}{F_\pi} g_A \left(1 + \Delta_{GT}\right) , \tag{12}$$

where

$$g_{\pi NN} = \frac{2 m_N}{m_\pi} f = 13.11 \pm 0.09 , \tag{13}$$

and $g_A = 1.2670 \pm 0.0035$ is the nucleon axialvector coupling constant (in units of g_V). With $F_\pi = 92.42 \pm 0.26$ MeV and $m_\pi = 139.570$ MeV we determine from (11) or (13) and (12) the *Goldberger-Treiman discrepancy*

$$\Delta_{GT} = \left(1.9 \pm 0.8\right) \times 10^{-2} . \tag{14}$$

In ChPT Δ_{GT} is given by [22]

$$\Delta_{GT} = -\frac{M_\pi{}^2}{8\pi^2 F_\pi{}^2 \cdot g_A} b_{19} , \tag{15}$$

where b_{19} is an LEC. With (14) we obtain from (15)

$$b_{19} = -0.9 \pm 0.3 , \tag{16}$$

which is of „natural size one". This represents a significant test of the chiral expansion.

These findings can be expressed alternatively, in the context of an objection raised by Stern and coworkers against the standard form of ChPT [26]. Stern et al. question the usual form of

ChPT which assumes that the masses of the light quarks (m_u, m_d, m_s) are sufficiently small. Specifically, they question the large value of the mass ratio

$$\frac{m_S}{\hat{m}} = 25.7 \pm 2.6 \qquad\qquad \hat{m} \equiv \left(\frac{m_u + m_d}{2}\right) \tag{17}$$

obtained by Gasser and Leutwyler [27] using standard ChPT. Stern et al. devised an alternative way for determining $m_S / \hat{m}$ – based on the Dashen-Weinstein sum rule – and obtained the upper limit

$$\frac{m_S}{\hat{m}} \leq 10.6 \pm 4.2 \ . \tag{18}$$

In the Dashen-Weinstein sum rule, the Goldberger-Treiman discrepancy, defined as

$$\delta_{\pi N} = F_\pi \cdot g_{\pi NN} - m_N \cdot g_A = (23 \pm 10)\,\text{MeV} \ , \tag{19}$$

is multiplied essentially with the ratio $m_S / \hat{m}$. (The value (19) follows from our result (13).) The limit (18) was obtained by using $\delta_{\pi N} = 66.0 \pm 8.5$ MeV – instead of (19). This means that (18) has to be multiplied by the factor 66/23 ≈ 2.9. Hence the objection of Stern et al. against standard ChPT is untenable.

Finally, we come to the (presently) rather controversial subject of the π*N sigma-term*[3)]. We are interested in the determination of the Σ-term from πN data.

The Σ-term is defined by means of the amplitude [28]

$$D(\nu, t) = A(\nu, t) + \nu \cdot B(\nu, t) \ , \tag{20}$$

where

$$\nu = \frac{s-u}{4m_N} \ ; \qquad \text{s, u: Mandelstam variables.}$$

$$\Sigma \equiv F_\pi^{\,2} \cdot \overline{D^+} \left(\nu = 0, \ \ t = 2m_\pi^{\,2}\right) \ , \tag{21}$$

where $\overline{D^+}$ is the isospin-even D amplitude from which the pseudovector Born term is subtracted, taken at the (unphysical) Cheng-Dashen point ($\nu = 0$, $t = 2m_\pi^2$). Some determinations of the Σ-term make use of the subthreshold expansion

$$\overline{D^+} \left(\nu, t\right) = d_{00}^+ + d_{01}^+ \cdot t + d_{02}^+ \cdot t^2 + d_{10}^+ \cdot \nu^2 + \ldots \tag{22}$$

---

3) See e.g. the various contributions to the MENU Symposium, Vancouver, BC, Canada, July 28 – August 1, 1997, in πN Newsletter, No. 13, Dec. 1998 (Eds.: D. Drechsel, G. Höhler, W. Kluge, H. Leutwyler, B.M.K. Nefkens, H.-M. Staudenmaier).

Inserting (22) in (21) we obtain to lowest order

$$\Sigma_d \;=\; F_\pi^{\,2}\left(d_{00}^{+} + 2m_\pi^{\,2}\cdot d_{01}^{+}\right) \tag{23}$$

so that

$$\Sigma \;=\; \Sigma_d \;+\; \Delta_D\;, \tag{24}$$

where Δ_D is due to the higher-order terms in (22).

Method	**Data**		**Σ_d [MeV]**	**Σ [MeV]**	**References**
hyperbolic dispersion relations	KH database			64 ± 8 ①	[29]
dispersion relations based on $b_0 \left(\equiv a_{0+}^{+}\right)$, a_{1+}^{+}	KH database		$50.0 \pm 3 \pm 8$ ②	62 ± 9	[30] [31]
	b_0 from the atoms	a_{1+}^{+} (KH)	$57.3 \pm 3 \pm 8$ ③		
		a_{1+}^{+} (SP98)	$65.8 \pm 3 \pm 8$ ④		[19]
		a_{1+}^{+} (ETL)	$54.0 \pm 3 \pm 8$ ⑤		[16] [23]
dispersion relations	VPI database		75.9 ⑥	92 ± 3 ⑥	[19]
ETL-model	KH database (low energy)			62.5 ± 5.5 ⑦	[32]
	$\pi^{\pm}p$ scattering ($20 < E_\pi < 100$ MeV)			74.8 ± 2.2 ⑧	[33] [16]

Table 3

In Table 3 we show determinations for both, Σ and Σ_d. The first determination ① was by Koch [29]. Gasser et al. [30] [31] devised a new analysis method in order to have a more realistic control on both, experimental and systematic errors. Experimental inputs are the s-wave scattering length b_0 and the p-wave scattering volume a_{1+}^{+}. Gasser et al. obtained the determination ② (± 3 MeV reflects the uncertainty of the input values and ± 8 MeV is systematic) from the Karlsruhe-Helsinki (KH) database. We can now use our new b_0 value in combination with various a_{1+}^{+} values and obtain the Σ_d determinations ③, ④, ⑤, using the analysis method of Gasser et al. We find an *increase in Σ_d of 7 MeV* (③-②) with respect to the old KH value ②. Recently, the VPI group with their SP98 solution obtained the very large values ⑥ for Σ_d and Σ [19]. The error assignment of 3 MeV is only part of the uncertainty in Σ [20]. It would be desirable to have realistic error estimates for the values ⑥.

An entirely different way of estimating the Σ-term is from the ETL-model (see sect. 3.1). With the (old) KH database, one obtains the value ⑦, and with the complete low-energy $\pi^{\pm}p$ elastic scattering data one finds the value ⑧. There seems to be an increase in Σ of 12 MeV (⑧-⑦) with respect to the (old) KH database (see sect. 4.3).

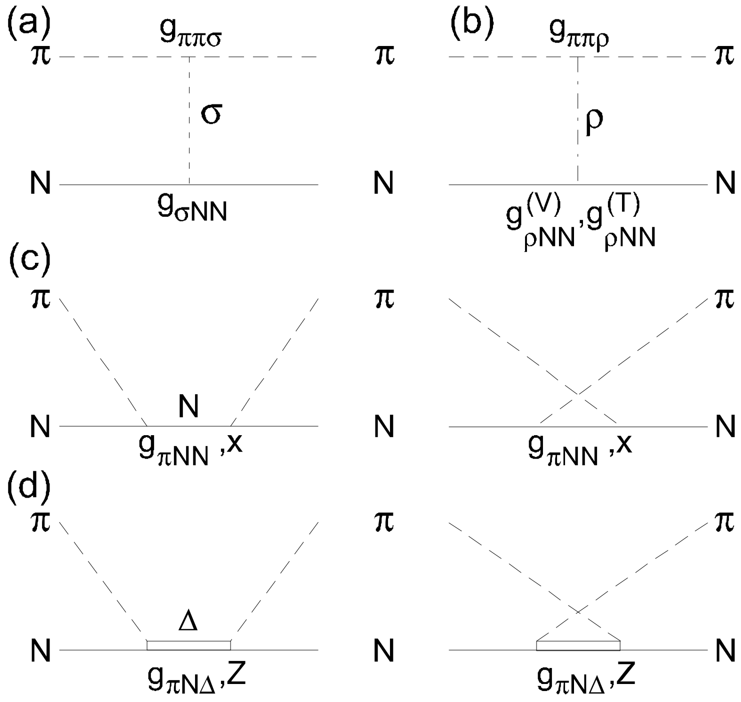

Fig. 10: The tree-level graphs of the ETL-model (see text).

3. Isospin-symmetry test from low-energy πN scattering [16]

3.1 The ETL-model of the πN interaction

The isospin-symmetry test of Matsinos [16] is based on the ETL-model [34] [35] [32]. The model is primarily designed to describe the πN interaction at *low energies* – exactly in the region where ChPT is supposed to work. (The model has also been used successfully up to the Δ_{33} resonance and beyond [36].) The unique features of the low-energy πN interaction are:

- The interaction is weak (phase shifts ≤ 6° for pion energies less then about 40 MeV);
- Higher partial waves (d, f, …) and contributions from resonances (other than Δ_{33}) are small;
- The range of the interaction is small compared to $\lambda_{deBroglie}$ and hence no form factors are needed.

In the low-energy limit of the model, the interaction is described by *all relevant tree graphs* (see Fig. 10). The scalar-isoscalar and the vector-isovector t-channel exchanges (a) and (b) are effective interactions. At low energies they are described by the three parameters

(a): $$G_\sigma = \frac{g_{\pi\pi\sigma} \cdot g_{\sigma NN}}{m_\sigma^{\,2}} \qquad (25)$$

(b): $$G_\rho^{(V)} = \frac{g_{\pi\pi\rho} \cdot g_{\rho NN}^{(V)}}{m_\rho^{\,2}} \ ; \qquad \kappa = \frac{g_{\rho NN}^{(T)}}{g_{\rho NN}^{(V)}} \quad , \qquad (26)$$

where m_σ, m_ρ are effective quantities; κ is the ratio between the tensor and the vector part. As a result of the conservation laws (including isospin), (a) and (b) are the only t-channel exchanges in the heavy-nucleon approximation. In addition, we have the s- and u-channel graphs

(c) and (d) with a nucleon and a Δ_{33} in the intermedial state. They are generally described by four parameters, namely

(c): $g_{\pi NN}$; x (isoscalar to isovector part)

(d): $g_{\pi N\Delta}$; Z (non-pole contributions).

These seven parameters describe nearly the most general isospin-symmetric low-energy πN interaction at the tree-level – except for possible derivative terms in the t-channel parts. At the $\pi\pi\sigma$ vertex in (a), the two lowest terms in a derivative expansion read

$$\Delta L_{\sigma\pi} = -g_{\pi\pi\sigma}\, m_\pi\, \vec{\pi}\cdot\vec{\pi}\,\Phi + \frac{h_{\pi\pi\sigma}}{m_\pi}\,\partial_\mu\vec{\pi}\cdot\partial^\mu\vec{\pi}\,\Phi\ , \tag{27}$$

where $\vec{\pi}$ is the pion field and Φ the scalar field.

Similarly, at the $\pi\pi\rho$ vertex in (b) the two lowest terms are of the form

$$\Delta L_{\rho\pi} = -g_{\pi\pi\rho}\ \vec{\rho}^{\,\mu}\left[\vec{\pi}\times\partial_\mu\vec{\pi}\right] - \frac{h_{\pi\pi\rho}}{2m_N^{\,2}}\left(\partial^\mu\vec{\rho}^{\,\nu} - \partial^\nu\vec{\rho}^{\,\mu}\right)\left[\partial_\mu\vec{\pi}\times\partial_\nu\vec{\pi}\right]\ , \tag{28}$$

where $\vec{\rho}^{\,\mu}$ is the vector field. The second term in (27) has been introduced by Matsinos [16]; considering the precision of the present data sets, its inclusion is not very important [37]. The second term in (28) has been investigated by Gridnev [36] in his extension of the ETL-model toward higher energies. With the present data sets there is no need for introducing the second term of (28).

The *K-matrix approach* is used in the ETL-model to extend the tree-level version towards higher energies and to unitarize (without introducing new parameters).

The seven parameters of the ETL-model are, in general, still too much freedom; as a rule, one obtains good fits to the data for every value of $G_\rho^{(V)}$ in the large range $(30 \le G_\rho^{(V)} \le 60)$ GeV^{-2}.

		$\mathbf{\frac{f^2}{4\pi}}$	**Reference**
	①	0.0757 ± 0.0010	eq. 11
	②	0.0760 ± 0.0005	[38]
ETL-model	③	0.0766 ± 0.0011	[16]
ETL-model	④	0.0738 ± 0.0011	[32]
	⑤	0.0790 ± 0.0010	[18]

Table 4

In order to demonstrate the successes of the ETL-model, I would like to discuss two examples, the *πN coupling constant* and the *Σ-term*. The first number ① for the πN coupling constant $f^2/4\pi$ in Table 4 is the value (11), i.e. from the atoms. Value ② is the recent dispersion-relation result of the VPI group, and ③ results from the ETL-model analysis of the low-energy $\pi^{\pm}p$ elastic scattering data. All three values are perfectly compatible. Also shown are two values deduced from the (old) KH database: ④ is again the parameter ($g_{\pi NN}$) of the ETL-model, and ⑤ is the original Karlsruhe-Helsinki value which has been criticized as being too high – even with respect to the KH database itself. Our value ④ is indeed lower and largely compatible with the three values based on the complete (modern) data set.

Now we come to the sigma-term. Within the tree-level version of the ETL-model, we obtain the very simple formula [34] [32]

$$\Sigma = F_\pi^{\,2}\left[\frac{2G_\sigma \cdot m_\pi}{1-2m_\pi^{\,2}/m_\sigma^{\,2}} - \frac{g_{\pi NN}^{\;2}}{m_N}\cdot\frac{x^2}{(1+x)^2}\right]. \tag{29}$$

The values ⑦ and ⑧ of Table 3 were obtained with formula (29). Both Σ-values which are deduced from the KH database (① and ⑦) are in perfect agreement. This shows that the simple formula (29) from the ETL-model is a valid estimate for the sigma-term (see also sect. 4.3).

3.2 Results

We come back to the isospin-symmetry test [16]. Matsinos has analyzed all elastic scattering- and SCX-data between 20 and 100 MeV pion energy with the (isospin-symmetric) ETL-model. It is useful to remember that the most general isospin-symmetric s- and p-wave πN amplitude can be written (in operator form) as

$$f_{\pi N} = \left[b_0(\varepsilon) + b_1(\varepsilon)\,\vec{\tau}\cdot\vec{t}\right] + \qquad \text{(s-wave)}$$

$$+ \left[c_0(\varepsilon) + c_1(\varepsilon)\,\vec{\tau}\cdot\vec{t}\right]\vec{k}_f\cdot\vec{k}_i +$$

(p-wave)

$$+ \left[d_0(\varepsilon) + d_1(\varepsilon)\,\vec{\tau}\cdot\vec{t}\right] i\vec{\sigma}\cdot\left(\vec{k}_f\times\vec{k}_i\right), \tag{30}$$

where

ε	: pion C.M. kinetic energy;	½ $\vec{\tau}$	: isospin of nucleon
$\vec{k}_i$, $\vec{k}_f$	: pion momenta;	½ $\vec{\sigma}$	: spin of nucleon
$\vec{t}$	: isospin of pion.		

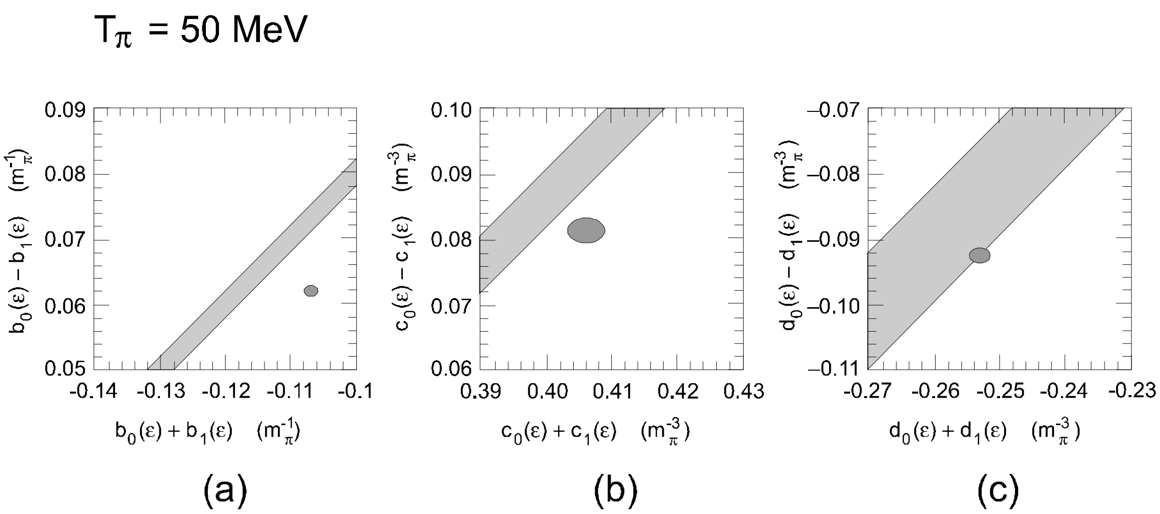

Fig. 11: Constraints on s- and p-wave coefficients of the πN interaction at 50 MeV pion energy [16]. The ellipses are from $\pi^{\pm}p$ elastic scattering data; the bands are from single charge exchange data: (a) s-wave; (b) p-wave, spin-independent part; (c) p-wave, spin-dependent part.

At each energy (e.g. T_π = 50 MeV) there are three amplitudes, each one being determined by two coefficients. An isospin-symmetry test is now represented with three figures (instead of the single Fig. 8 at threshold), one for each amplitude (see Fig. 11). Any pair of linearly independent coefficients (real parts) of (30) can be plotted. The coefficients plotted in Fig. 11 correspond to the π^+p elastic-scattering channel (sum of coefficients) and to the π^-p elastic-scattering channel (difference of coefficients), respectively. Matsinos has analyzed the data in two groups: all $\pi^{\pm}p$ elastic scattering data in one group and the SCX data in the other. The ellipses in Fig. 11 are the one-standard-deviation contours of the solutions from the $\pi^{\pm}p$ group, and the inclined bands correspond to the one-standard-deviation constraints from the SCX group. Isospin symmetry of the πN interaction at the particular energy (50 MeV in our case) implies compatibility between ellipses and bands. There is clear evidence for isospin-symmetry violation at least in the s-wave (around T_π = 50 MeV) – provided (of course) that

i) the ETL-model is a complete description of an (isospin symmetric) πN interaction;

ii) the electromagnetic corrections which were applied [39] are correct.

We will discuss both these points in sects. 4.2 and 4.3.

4. Summary

4.1 Pionic hydrogen experiments

1. From the measured shifts of the 1s states in the (π^-p)- and (π^-d)-atoms and the 1s width in the (π^-p)-atom, we determine the πN scattering lengths (assuming isospin symmetry)

$$b_0 = (1.6 \pm 1.3) \times 10^{-3} m_\pi^{-1} ; \qquad b_1 = -(86.8 \pm 1.4) \times 10^{-3} m_\pi^{-1} .$$

   The present limitations are the three-body calculations in the (π^-d)-system.

2. The isovector scattering length b_1 – using the GMO sum rule – leads to a new value for the πN coupling constant:

$$\frac{f^2}{4\pi} = 0.0757 \pm 0.0010\,; \qquad\qquad g_{\pi NN} = 13.11 \pm 0.09\,.$$

3. From the πN coupling constant we determine the Goldberger-Treiman discrepancy

$$\Delta_{GT} = (1.9 \pm 0.8) \times 10^{-2}.$$

4. The isoscalar scattering length b_0 implies an increase in the πN sigma-term (Σ_d) by 7 MeV with respect to the KH value.

5. The scattering lengths b_0, b_1 are dominated by the first-order term (current-algebra limit) of the ChPT expansion.

4.2 Electromagnetic corrections

The electromagnetic corrections for pionic hydrogen (π^-p) are known at the 0.5% level [7]. They are relatively small (switching the corrections off completely would move the ellipse in Fig. 8 to the doted position.) The complete electromagnetic corrections for pionic deuterium are still missing and should be considered in the context of improved (three-body) calculations relating the π^-d scattering length to the πN system.

The electromagnetic corrections in most [4)] analyses of scattering experiments are those of Tromborg et al. [39]. The concept is compatible with the one used in ref. [7] for pionic hydrogen. The mass-splitting correction of Tromborg has recently been improved by Gridnev [36], incorporating the Δ_{33} mass-splitting effect. The change with respect to Tromborg's correction in the low-energy regime is small (but not in the resonance region). Tromborg's procedure is critically examined presently at the University of Zürich [40]. For the following discussion, I assume Tromborg's corrections to be valid in the low-energy regime and the missing electromagnetic corrections for the (π^-d)-system to be small.

4.3 The ETL-model, isospin symmetry, and sigma-term

There are two signatures for isospin-symmetry breaking. One is the difference between our b_1 value and b_1 (M) (the square in Fig. 8) which is the projection to threshold of the ETL-model solution based on $\pi^{\pm}p$ elastic scattering. The other is the incompatibility between the SCX data near 50 MeV and the $\pi^{\pm}p$ elastic scattering data, both analyzed with the ETL-model (Fig. 11 (a)). The latter signature could also be accounted for by a modification of the isovector s-wave coefficient $b_1(\varepsilon)$ (by 6.4 ± 1.4%).

Could it be that the ETL-model has a small missing piece which would mainly modify the isovector coefficient $b_1(\varepsilon)$ at low energies? From the construction of the model (sect. 3.1) it is clear that an additional (isospin-symmetric) contribution must come from non-tree-level graphs which contribute around (and below) threshold; such a graph is depicted in Fig. 12. Contributions from this graph would also modify the formula (29) for the sigma-term. In or-

---

[4)] Different procedures are used by the VPI group.

der to assess the amount of explicit isospin-symmetry breaking and to improve the value of the sigma-term it is therefore highly desirable to estimate the contributions from the graph of Fig. 12.

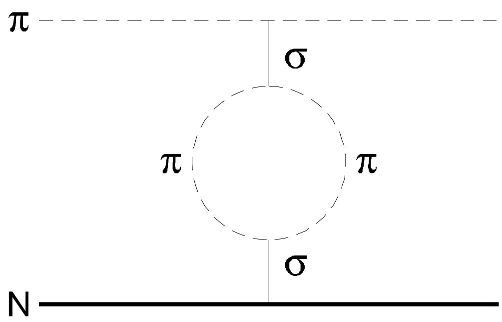

Fig. 12: Graph which is not contained in the ETL-model of the πN interaction.

Some general comments on the ETL-model are appropriate here. The ETL-model (in its present form) provides an extremely useful and powerful link between experiment and theory. The reasons are:

- The model provides a description of the low-energy πN interaction in terms of only six or seven, physically significant parameters (coupling constants, mixing parameters etc.).

- The model is (by construction) designed to describe the low-energy end of the πN interaction – exactly the region where ChPT is supposed to work best.

- In contrast to dispersion-relation techniques, cross-section data from the high-energy resonance region enter only weakly.

For these reasons, the ETL-model (with its intrinsic simplicity) is an important complement to the more complex dispersion relation methods. The model has built in the fact that the πN interaction is weak at low energies (tree-level limit). This leads to the small number of free parameters and hence to inherently precise results.

We summarize:

6. The (possibly improved) ETL-model is an important tool [5)] for investigating
   - isospin-symmetry breaking,
   - the sigma-term puzzle,
   - the convergence properties of ChPT [41],

   and for determining the LEC's of ChPT.

[5)] In electromagnetic corrections for πN scattering, potentials to account for the strong interaction are sometimes used [40]. These potentials are not unique; the ETL-model could be used to constrain them.

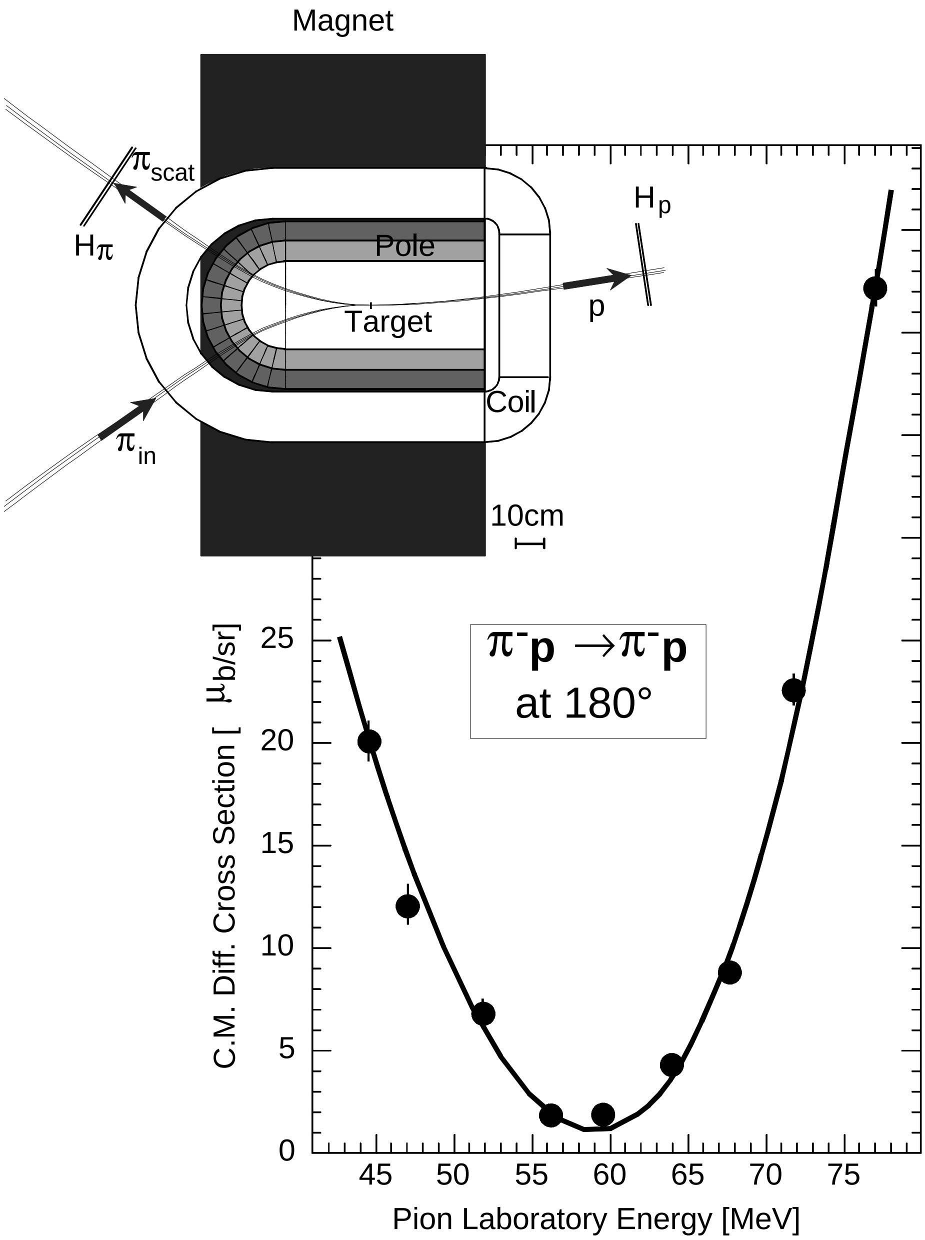

Fig. 13: Destructive interference of s- and p-waves in 180° $\pi^- p$ elastic scattering [42]; experimental layout and differential cross section as a function of pion energy (preliminary data from improved experiment).

5. A new experiment [42]

Fig. 13 shows the differential cross section in backward $\pi^- p$ elastic scattering (scattering angle 180°), measured as a function of the incident pion energy. We observe an unusual behavior: At the *„magic energy"* (near 60 MeV) the cross section is nearly zero and rises steeply and symmetrically around that energy.

The explanation of this phenomenon is as follows. At the scattering angle of 180°, the nucleon spin term in the amplitude (30) vanishes. In the energy range considered, the coefficients of $f_{\pi N}$ are nearly real and the s- and p-waves dominate. The (real part of the) s-wave amplitude varies slowly with energy, while the p-wave part is approximately proportional to $\vec{k}^2$. At the magic energy the two cancel exactly, giving rise to the zero in the cross section: The pronounced dip is the result of *destructive interference* between the s- and p-wave amplitudes.

Apart from being a beautiful textbook experiment for demonstrating quantum-mechanical interference, the experiment is also of great practical importance. Since the dominant parts of the amplitude cancel, the experiment is particularly sensitive to small parts of the interaction – such as *isospin-symmetry breaking* pieces. It so happens that the s-wave amplitude ($b_0(\varepsilon)$ - $b_1(\varepsilon)$) is dominated by $b_1(\varepsilon)$ ($b_0(\varepsilon)$ is still small at these energies). The π^-p destructive interference experiment should therefore provide new and precise information on the important isovector coefficient $b_1(\varepsilon)$ (sect. 4.3). – The data analysis of an improved version of the experiment is in progress.

6. Outlook

6.1 Isospin breaking

There are two ways of further quantifying the amount of isospin-symmetry breaking. One is to estimate the contributions of non-tree graphs to the ETL-model (sect. 4.3), and then use them as corrections to the model in the analysis around 50 MeV [16] and also for the extrapolation of $\pi^{\pm}p$ analysis to threshold (sect. 2.2). Any remaining incompatibility (around 50 MeV or at threshold) would have to be assigned to isospin-symmetry breaking of the strong interaction.

The other way is to form a database from all $\pi^{\pm}p$ elastic scattering results – including b_0, b_1 from the hydrogen experiments – and perform a partial-wave dispersion-relation analysis (always implementing isospin symmetry). Given that there is compatibility with the database, SCX-scattering cross sections could be predicted from this analysis and compared e.g. with the experiment of Fitzgerald et al. [43]. In this scheme the Fitzgerald-experiment, which is also based on destructive interference, plays the key role. An (improved) repetition of the Fitzgerald-experiment is therefore highly desirable and is, in fact, underway [44]. It is also the key-experiment for the isospin effect of ref. [16].

6.2 The strong-interaction pion mass

The quantity of great physics interest in the ChPT of the πN interaction is the expansion parameter $M_\pi \equiv M_{\pi^+}$, the *strong-interaction pion mass* which – in the isospin-symmetry limit – is single-valued. M_π contains the u- and d-quark-mass dependence and is given in QCD by the exact relation [1] [6)]

$$M_{\pi+}^{\;2} = \left(m_u + m_d\right) \frac{G_\pi}{F_\pi} , \tag{31}$$

where G_π is proportional to the matrix element of the pseudoscalar density $\langle \pi^+ | \bar{u}\, \gamma_5\, d | 0 \rangle$ and F_π is the pion decay constant (quantity proportional to the corresponding matrix element of the pseudovector density). *It should be possible, in principle, to determine M_π from the πN data by treating M_π in the ChPT expansion as a free parameter* (along with the LEC's). Theo-

6) M_π differs from the charged–pion mass (m_π) through the electromagnetic contributions.

retically, one expects the difference between (measured) charged and neutral pion mass to be due entirely to the electromagnetic interaction [45]. Therefore M_π should certainly be different from the measured charged pion mass (m_π).

A practical determination of M_π from the πN data set should probably proceed iteratively. One must realize that all electromagnetic corrections calculated so far have been done by *conventionally* assigning m_π as the strong-interaction pion mass. (This holds for the electromagnetic corrections calculated for pionic hydrogen [7], as well as for the procedure of Tromborg [39] which is most frequently used in πN scattering.) Conceptually, the isospin symmetry problem (sect. 6.1) should be solved first because, if isospin-symmetry is broken sizably, then the ChPT expansion contains an additional parameter, depending on the u- and d-quark mass *difference*.

Acknowledgments

This work has gained from discussions with Andreas Badertscher, Thomas Becher, Markus Janousch, Joachim Kambor, Heinrich Leutwyler, Nadia Fettes, Peter Goudsmit, Anatoli Gridnev, Evangelos Matsinos, Ulf Meissner, Peter Weber, and Daniel Wyler.

REFERENCES

[1] H. Leutwyler, in Chiral Dynamics: Theory and Experiment, Springer (1995), A. M. Bernstein and B. R. Holstein (Eds.), p. 14.

[2] D. Sigg et al., Phys. Rev. Lett. *75* (1995) 3245.

[3] D. Sigg et al., Nucl. Phys. *A 609* (1996) 269; Erratum *A 617* (1997) 526.

[4] H.-Ch. Schröder et al., in preparation; H.-Ch. Schröder, Diss. ETH No. 11760 (1996).

[5] D. Chatellard et al., Phys. Rev. Lett. *74* (1995) 4157.

[6] D. Chatellard et al., Nucl. Phys. *A 625* (1997) 855.

[7] D. Sigg et al., Nucl. Phys. *A 609* (1996) 310.

[8] E. Bovet et al., Nucl. Instrum. Methods *190* (1981) 613.

[9] A. Foster et al., Phys. Rev. *C 28* (1983) 2374.

[10] E. Bovet et al., Phys. Lett. *B 153* (1985) 231.

[11] W. Beer et al., Phys. Lett. *B 261* (1991) 16.

[12] J. Bailey et al., Phys. Lett. *B 50* (1974) 403.

[13] A. W. Thomas and R. H. Landau, Phys. Rep. *C 58* (1980) 122.

[14] A. Badertscher et al., ETHZ-IPP preprint PR-94-10; H. J. Leisi et al., in Chiral Dynamics: Theory and Experiment, A. M. Bernstein and B. R. Holstein (Eds.), Springer (1995), p. 241.

[15] P. B. Siegel and W. R. Gibbs, Phys. Rev. *C 33* (1986) 1407.

[16] E. Matsinos, Phys. Rev. *C 56* (1997) 3014.

[17] N. Fettes and E. Matsinos, Phys. Rev. *C 55* (1997) 464.

[18] R. Koch and E. Pietarinen, Nucl. Phys. *A 336* (1980) 331; R. Koch, Nucl. Phys. *A 448* (1986) 707.

[19] R. A. Arndt et al., πN Elastic scattering analysis and dispersion relation constraints, nucl-th/9807087 Jul 1998, submitted for publication to Phys. Rev. C.

[20] M. M. Pavan, private communication (September 28, 1998).

[21] J. Gasser, M. E. Sainio and A. Svarc, Nucl. Phys. *B 307* (1988) 779.

[22] M. Mojzis, Euro. Phys. J. *C2* (1998) 181.

[23] N. Fettes, U.-G. Meissner and S. Steininger, Nucl. Phys. *A 640* (1998) 199.

[24] M. L. Goldberger, H. Miyazawa, and R. Oehme, Phys. Rev. *99* (1955) 986.

[25] R. L. Workman, R. A. Arndt, and M. M. Pavan, Phys. Rev. Lett. *68* (1992) 1653.

[26] N. H. Fuchs, H. Sazdjian and J. Stern, Phys. Lett. *B 238* (1990) 380.

[27] J. Gasser and H. Leutwyler, Phys. Rep, *87* (1982) 77; Ann. Phys. (NY) *158* (1984) 142; Nucl. Phys. *B 250* (1984) 465, 517, 539.

[28] G. Höhler, in Landolt-Börnstein, Vol. 9 b2, ed. H. Schopper (Springer, Berlin, 1983).

[29] R. Koch, Z. Phys. *C 15* (1982) 161.

[30] J. Gasser, H. Leutwyler, M. P. Locher, and M. E. Sainio, Phys. Lett. *B 213* (1988) 85.

[31] J. Gasser, H. Leutwyler, and M. E. Sainio, Phys. Lett. *B 253* (1991) 252.

[32] P. F. A. Goudsmit, H. J. Leisi and E. Matsinos, B. L. Birbrain and A. B. Gridnev, Nucl. Phys. *A 575* (1994) 673.

[33] E. Matsinos, Workshop on the Low-Energy Pion-Nucleon Interaction, ETH Zürich / PSI, September 8 - 9, 1997 (unpublished).

[34] P. F. A. Goudsmit, H. J. Leisi, and E. Matsinos, Phys. Lett. *B 299* (1993) 6.

[35] P. F. A. Goudsmit, H. J. Leisi, and E. Matsinos, Helv. Phys. Acta *67* (1994) 369.

[36] A. B. Gridnev, The mass splitting corrections to pion-nucleon scattering in the tree-level K-matrix approach, preprint ETHZ-IPP PR-97-07, and private communication (1997).

[37] E. Matsinos, private communication (1997).

[38] M. M. Pavan and R. A. Arndt, MENU Symposium, Vancouver, BC, Canada, July 28 - August 1, 1997, in πN Newsletter, No. 13, Dec. 1998 (Eds.: D. Drechsel, G. Höhler, W. Kluge, H. Leutwyler, B. M. K. Nefkens, H.-M. Staudenmeier), p. 165.

[39] B. Tromborg et al., Phys. Rev. *D 15* (1977) 725; Helv. Phys. Acta *51*, (1978) 584.

[40] G. Rasche, E. Matsinos, private communication (1998).

[41] H. Leutwyler, private communication (1997). Also compare footnote [20] of ref. [1].

[42] M. Janousch et al., Phys. Lett. *B 414* (1997) 237; P. F. A. Gondsmit et al., preprint ETHZ-IPP PR-95-2.

[43] D. H. Fitzgerald et al., Phys. Rev. *C 34* (1986) 619.

[44] J. Comfort, private communication (1998).

[45] J. Gasser and H. Leutwyler, Phys. Rep. *C 87* (1982) 77.